

Incidence Angle Resolved Scattering for Optical Characterization of Thin Films

Peter J. Dudenas^{a,b*}, Adam Z. Weber^b, and Ahmet Kusoglu^b

^aChemical and Biomolecular Engineering, University of California, Berkeley, CA 94720 USA

^bEnergy Conversion Group, Lawrence Berkeley National Lab, CA 94720 USA

Abstract

Grazing incidence x-ray scattering provides nanostructural information for thin film systems, but single images do not provide information on film thickness or the full complex index of refraction. X-ray reflectivity is a complementary technique that can provide this information, but it is most often done ex-situ. In this paper, we present an *in-situ* method to extract these parameters using scattering images taken across a range of incident angles. We validate the technique using a set of polymer thin films and discuss how it can be implemented as a general beamline procedure.

Introduction

Grazing incidence x-ray scattering has become a routine characterization method to determine the nanostructure morphology of thin films. Third generation synchrotron sources have the x-ray flux and detector technology necessary to provide high-throughput environments in which researchers can shoot their samples quickly and efficiently. Often the limiting step in publishing this research is data interpretation and modeling, which is made more complicated due to dynamical scattering. This often makes it necessary to model data within the Distorted Wave Born Approximation (DWBA). A number of groups have put forth significant efforts and released programs to model scattering data, including IsGISAXS[1], BornAgain[2], and HiPGISAXS[3] (among others), significantly reducing the barrier for researchers to model their data. Nonetheless, modeling is often still a challenging and computationally expensive process. Additionally, Fresnel coefficients for each layer of the sample are required for modeling, which are calculated once the complex index of refraction and thickness of each layer are known. For complicated samples with multiple layers, or environmentally sensitive (i.e. hygroscopic, oxygen sensitive) samples, this can be a challenge or may change from the beamline to ex-situ characterization. Incidence angle resolved (IAR) scattering provides a method to determine the optical constants of a sample in-situ, as well as depth-sensitive information to constrain further modeling and data analysis.

In this paper, we summarize the relevant theory

for grazing incidence scattering and optics, and then demonstrate how the specular rod intensity as a function of incidence angle can be used to determine the complex index of refraction and film thickness of a sample. Furthermore, we outline how this procedure could be automated at the beamline to help researchers more intelligently decide at which incidence angles to shoot.

Background/Theory

A large body of literature exists covering theory of the DWBA scattering cross-section in grazing-incidence geometry for both x-ray and neutron scattering[4–8]; we briefly outline general results here. The total scattering cross-section for a rough film is shown below in equation 1[9].

$$\frac{\partial\sigma}{\partial\Omega} = \left(\frac{\partial\sigma}{\partial\Omega}\right)_{Fresnel} e^{-Q_z^2\sigma^2} + \left(\frac{\partial\sigma}{\partial\Omega}\right)_{diffuse} \quad (1)$$

The first term in equation 1 is the specularly reflected x-ray beam, which, subtending some solid angle on a point detector, is what is measured in x-ray reflectivity experiments. Often, this is blocked in grazing incidence x-ray experiments to prevent the intense specular reflection from damaging the area detector. The second term in equation 1 is the diffuse scattering cross section, which includes scattering due to surface roughness, and scattering from any structures present in the film. DWBA modifies the diffuse scattering cross-section, accounting for multiple scattering.

The observed scattering intensity is proportional to

this diffuse scattering cross-section, multiplied by the electric field intensity (EFI). The EFI is very sensitive to the incidence angle, and can vary greatly with depth through the film. This phenomena is due to x-ray waveguiding, and its depth-dependence has been used to elucidate positions of nanoparticles within polymer thin films[10–13]. Jiang et al. importantly detailed how EFI affects the observed scattered intensity, and how to self-consistently calculate the cross-section using a slicing algorithm[14, 15]. More recently, x-ray waveguiding has been applied to reveal stratification of crystallite orientation in semi-conducting polymer thin films[16].

A sample's EFI at a given angle is dependent on the optical properties (complex index of refraction) and thickness of the layers that comprises the sample. EFI can be calculated from Equation 2

$$EFI = |T_j e^{ik_{z,j}z} + R_j e^{-ik_{z,j}z}|^2 \quad (2)$$

Where T_j , R_j are the complex transmitted and reflected wave amplitudes, and $k_{z,j}$ is the z-component of the wave vector within layer j. To determine these values throughout the film, we use Parratt's recursion[15], as laid out in M. Tolan's monograph *X-Ray Scattering from Soft-Matter Thin Films*[17]. These equations are derived for s-polarized x-rays, as typically produced by synchrotron bending magnets and undulators.

A sample is divided into N+1 layers, and the ratio of reflected to transmitted waves is calculated via Equation 3

$$X_j = \frac{R_j}{T_j} = e^{-2ik_{z,j}z_j} \frac{r_{j,j+1} + X_{j+1} e^{2ik_{z,j+1}z_j}}{1 + r_{j,j+1} X_{j+1} e^{2ik_{z,j+1}z_j}} \quad (3)$$

where

$$r_{j,j+1} = \frac{k_{z,j} - k_{z,j+1}}{k_{z,j} + k_{z,j+1}} \quad k_{z,j} = k (n_j^2 - \cos^2 \alpha_i)^{\frac{1}{2}}$$

n_j is the complex index of refraction in layer j, α_i is the incidence angle, and k is the x-ray wave vector in vacuum. $r_{j,j+1}$ is the Fresnel reflection coefficient at the interface between layers j and j+1. The substrate is assumed to be thick enough such that no reflections occur and $R_{N+1} = 0$. Starting at j=N, X_j is calculated recursively up to layer j = 1, where T_1 has been normalized to 1 and so $X_1 = R_1$ is known. $|R_1|^2$ is the specular reflection as measured in traditional x-ray reflectivity experiments.

Using equations 4 and 5, the complex wave amplitudes through the rest of the film can be calculated

$$R_{j+1} = \frac{1}{t_{j+1,j}} \left[T_j r_{j+1,j} e^{-i(k_{z,j+1} + k_{z,j})z_j} + R_j e^{-i(k_{z,j+1} - k_{z,j})z_j} \right] \quad (4)$$

$$T_{j+1} = \frac{1}{t_{j+1,j}} \left[T_j e^{i(k_{z,j+1} - k_{z,j})z_j} + R_j r_{j+1,j} e^{i(k_{z,j+1} + k_{z,j})z_j} \right] \quad (5)$$

where

$$t_{j+1,j} = 1 + r_{j+1,j}$$

Surface roughness can be incorporated via the Fresnel coefficients, and the procedure is outlined further in the above text[17].

Calculating the EFI through a film as a function of incidence angle leads to EFI maps as shown in Figure 1.

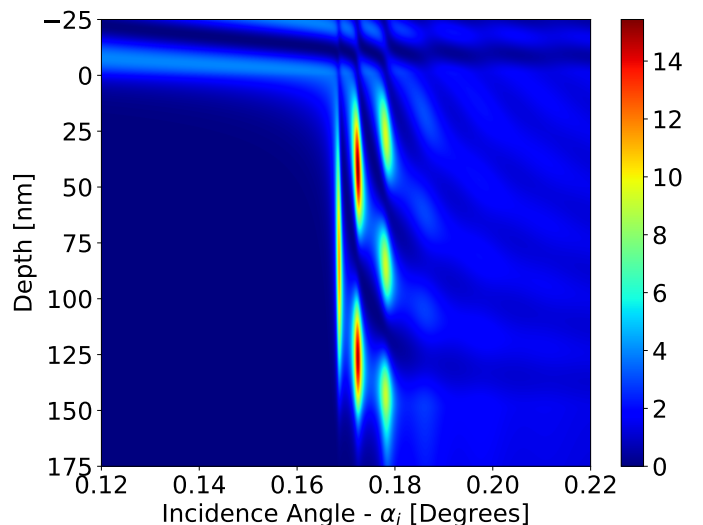


Figure 1: Electric Field Intensity map for a 150 nm Nafion Film

At specific incidence angles, the incoming x-ray beam couples into the film, leading to transverse electric resonance modes and large EFI enhancement at certain depths within the film. These angle- and depth-dependent EFIs are what allow researchers to determine the z-position of specific scatterers within a sample. Rather than looking at scatterers within the film, we instead focus here on scattering intensity that comes from surface roughness at the film-air interface.

Roughness at the film-air interface causes the incoming x-ray beam to be scattered/reflected with some small change in q_x and q_y , resulting in a bright rod on the detector; this is often referred to as the specular rod. Figure 2 compares the reflectivity and surface EFI curves versus incidence angle.

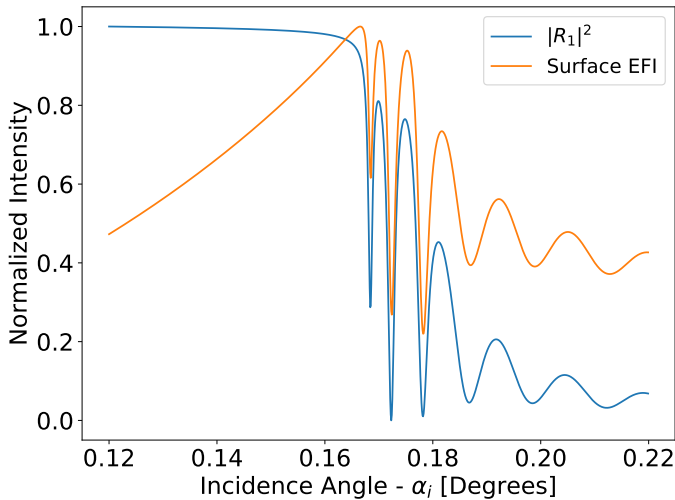


Figure 2: Reflectivity and Surface EFI for the 150 nm Film in Figure 1

Just as the scattering from objects within the film is proportional to the EFI at that position, the specular rod intensity is proportional to the EFI at the film-air interface. This is in contrast to the specular x-ray reflectivity, which is proportional only to the squared modulus of the reflected wave amplitude. To construct surface EFI plots, a portion of the specular rod intensity is integrated at each angle to generate the data and care is taken to choose a portion of the specular rod that does not overlap with other sources of strong diffuse scattering. Once the spectra has been collected, modelled EFI data can be calculated as outlined above. This can be embedded within a fitting procedure where the complex index of refraction, thickness, and surface roughness are the fitting parameters. For multilayer systems, this can be generalized to include each layer. Optical constants estimated using the CXRO database[18] provide a good starting point for the fitting parameters.

Effect of Beam Divergence and Energy Resolution

The EFI map and curves in Figures 1 and 2 are calculated assuming a monochromatic plane wave. At a real beamline, sources will have a finite angular divergence and energy resolution. Depending on the magnitude of these values, they may need to be accounted for. These effects are demonstrated using parameters from Beamline 7.3.3 at the Advanced Light Source[19]. 7.3.3 uses a pair of multilayer mirrors as their monochromator, where each mirror is 250 multilayers of alternating B_4C and Mo . The multilayer period is 2 nm ($\Gamma=0.5$) and the monochromator is operated at 10 keV ($\lambda=1.24 \text{ \AA}$),

with an incidence angle of 1.794 degrees (1st multilayer Bragg angle). The dE is ~ 100 eV and the full energy spectrum is shown in Figure 3.

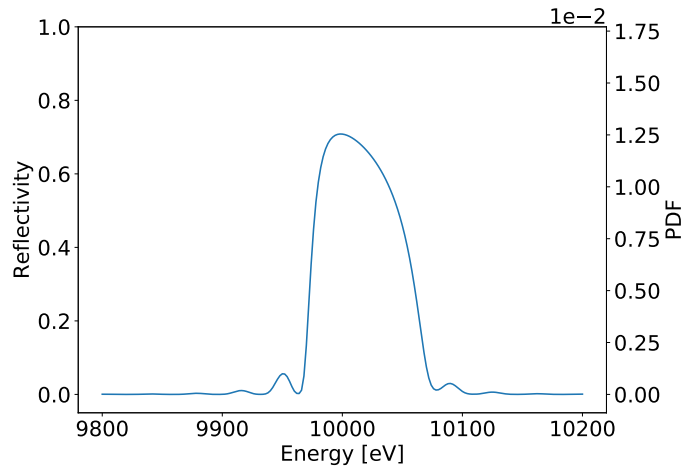


Figure 3: Energy spectrum at Beamline 7.3.3, shown both as reflectivity and normalized probability distribution

To calculate the effect of finite energy resolution, EFI maps at each energy are calculated and then summed, weighted by the energy spectrum PDF. Correspondingly, the index of refraction for the film and substrate must also be adjusted for each energy. Figure 4 shows the real and imaginary parts of the index of refraction for the silicon substrate and Nafion thin film (Nafion is an ion-conducting polymer commonly used in fuel cells), calculated from CXRO.

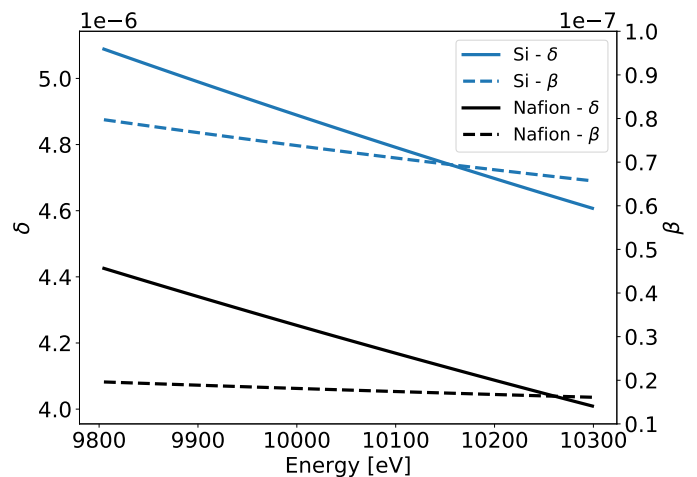


Figure 4: Optical constants for silicon and Nafion versus energy calculated from CXRO

Even with a perceived large dE/E of 0.1, the effect of energy resolution is small on the resulting EFI spectrum (Figure 5) and neglected in further calculations. Energy resolution may be more important at lower x-ray energies, where the index of refraction changes more rapidly with energy.

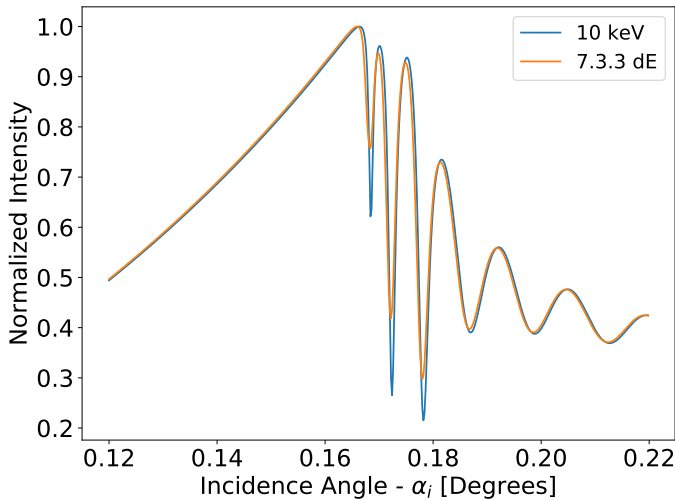


Figure 5: Surface EFI versus incidence angle for monochromatic 10 keV x-rays and finite energy resolution using the energy spectrum shown in Figure 3

The second effect that may need to be accounted for is angular divergence of the beam; at 7.3.3 this is quoted at 2.78 mrad. Assuming a gaussian distribution, the divergence is accounted for by convolving the EFI for a plane wave with a gaussian distribution in incidence angle (Figure 6). Unlike energy resolution, the angular divergence does have a significant effect, and will be included in subsequent calculations.

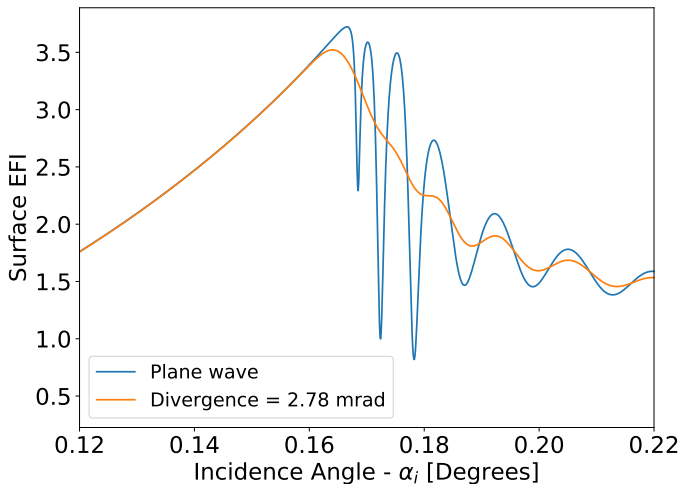


Figure 6: Surface EFI versus incidence angle for a plane wave and gaussian beam at 10 keV

Experimental Results and Discussion

Nafion thin films were cast at 10 different thicknesses and sets of GIWAXS images were taken at incidence angles from 0.12° - 0.25° . At each incidence angle, a small portion of the specular rod intensity is averaged to create intensity versus incidence angle plots. Surface EFI calculations are then fit to the data. Figure

7 shows a representative set of experimental data and the EFI fit.

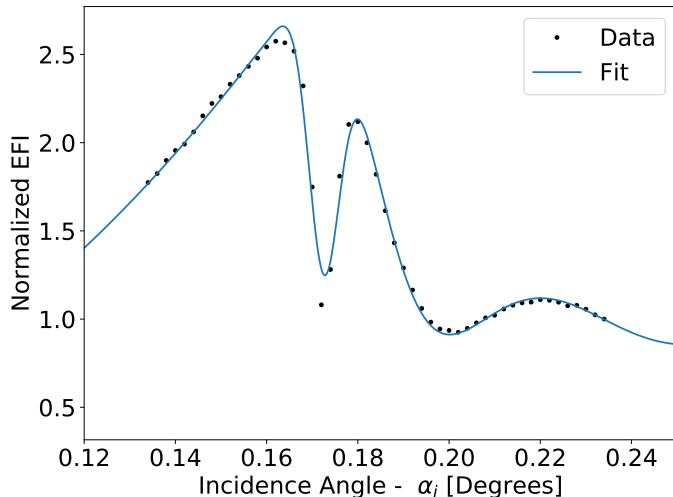


Figure 7: Experimental data and fit EFI curve for a 47 nm film.

Film thickness, delta, beta, surface roughness, and a scaling constant are fitting parameters. Additionally, the sample alpha alignment procedure at 7.3.3 introduces uncertainty into the recorded incidence angle and may shift curves by up to 0.02° . Fitting is repeated at multiple angle offsets to find a minimum in the mean squared error. Plotted in Figure 8 is the film thickness extracted from fitting versus film thickness measured via ellipsometry. Across an order of magnitude in film thickness, there is excellent agreement between the two techniques.

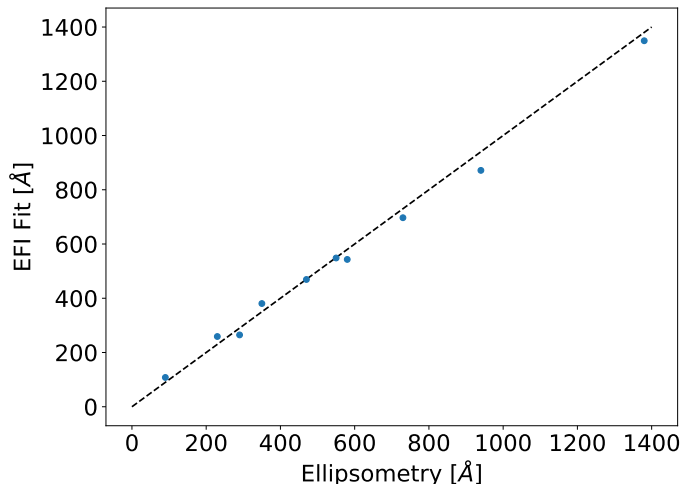


Figure 8: Film thickness from EFI fit versus film thickness measured using ellipsometry. Dotted line has a slope of 1

Continuing, the real and imaginary parts of the index of refraction are plotted versus film thickness in Figure 9. δ shows reasonable trends with film thickness, but β displays a considerable spread. This spread

is likely aphysical and will need to be validated against specular x-ray reflectivity measurements. The effect of macroscopic thickness variation has not been considered here but may play a role. Furthermore, the 2.78 mrad beam divergence is measured before a number of optical elements at 7.3.3 and may be different where the sample sits.

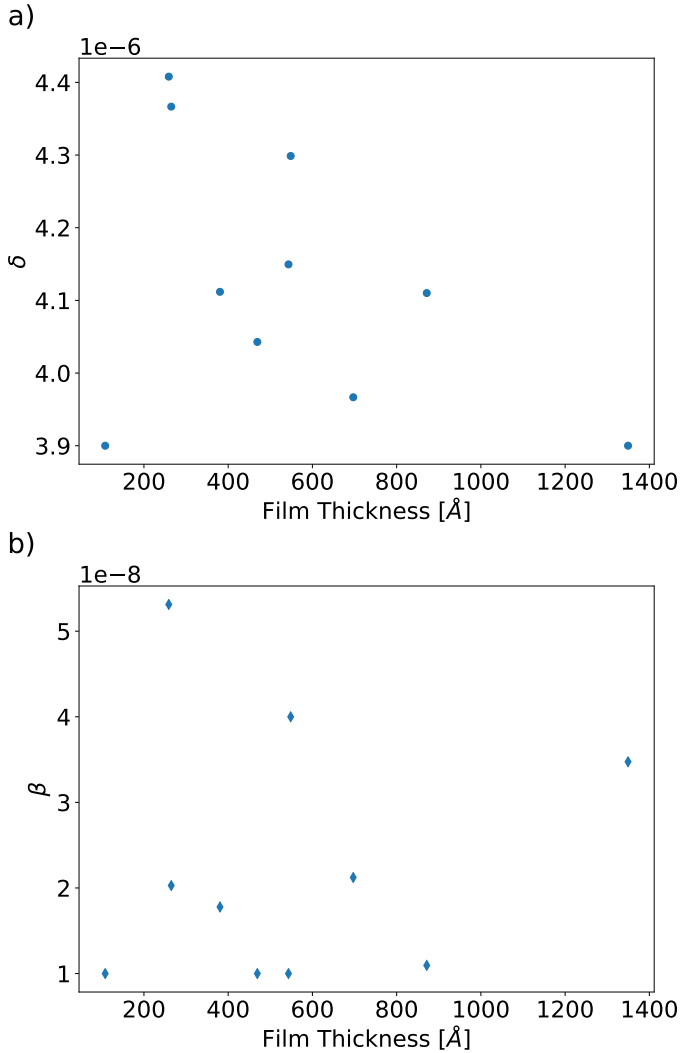


Figure 9: Extracted a) real and b) imaginary parts of the index of refraction versus film thickness. β 's large spread and lack of trends with thickness indicate an aphysical result. The estimated δ and β for bulk Nafion at 10 keV is 4.25×10^{-6} and 1.81×10^{-8} , respectively

Because this optical characterization is done *in-situ*, it is advantageous for temporal experiments and environmentally sensitive samples. As an example, Nafion is a hygroscopic material that is very sensitive to relative humidity (RH). Grazing incidence experiments that control RH *in-situ* can also track film thickness and index of refraction, connecting macroscopic properties and swelling to nanostructural morphology changes in one experiment. Additionally, any modeling

using DWBA will benefit from the additional information gained through this technique.

Beamline Procedure

For weakly scattering polymer samples such as Nafion, the signal of the specular rod can be 100 times more intense than from structures within the film, allowing for short exposure times to generate the IAR data. This could be translated into a beamline control plugin: A region of interest (ROI) is selected on the detector over which to integrate intensity. An alpha scan is then performed at short exposure times ($O(0.1 \text{ s})$), integrating the ROI, and returning the IAR data to the user. From these plots, critical angles and TE modes are easily identified, and the researcher can make a more informed decision on which incidence angles to collect longer exposures. In the end, this strategy can potentially reduce the number of long exposure images, mitigating beam damage and time spent on each sample.

In order for this technique to be successfully applied, a few conditions should be met. The first requirement is an x-ray source of small angular divergence. As the angular divergence increases, the EFI is smeared, resulting in smaller signal enhancement and modulation. With 3rd generation synchrotron x-ray sources, this criteria should be satisfied. The second criteria recommended is a goniometer with uncertainty in the incidence angle of less than $\sim 5\%$ ($\sim 0.01^\circ$ for 10 keV). The real part of the index of refraction is very sensitive to shifts in the incidence angle. If this precision cannot be met, an alternative strategy is to use the substrate's Yoneda peak as an internal standard for the calculating the incidence angle of each image. Finally, the ROI for integration must be free from other strong sources of diffuse scattering within the film. Otherwise the integrated intensity will be a function of EFI at both the surface and where the additional scattering sources reside within the film.

Conclusion

In this paper we review a method to calculate recursively the electric field intensity (EFI) of x-rays in thin films and discuss how the specular rod in grazing incidence x-ray experiments is proportional to EFI at the film-air interface. We compare surface EFI to specular reflectivity and explore the effects of angular divergence and energy resolution. Applying these principles, we demonstrate how incidence angle resolved scatter-

ing can be used to extract optical constants and film thickness from Nafion polymer thin films ranging from 100 - 1400 Å. The advantages and limitations of the technique are discussed, including necessary beamline criteria. Incidence angle resolved scattering is a general technique, enabling *in-situ* optical characterization for any thin film system.

Acknowledgements

The authors would like to thank Zhang Jiang, Chenhui Zhu, and Alex Hexemer for helpful discussions. The authors would also like to thank Alastair MacDowell for providing the multilayer monochromator specifications. PJD acknowledges support from the Army Research Office under award number AWD00000675. This research used beamline 7.3.3 of the Advanced Light Source, which is a DOE Office of Science User Facility under contract no. DE-AC02-05CH11231.

Author Information

*Corresponding Author: pete.dudenas@berkeley.edu

References

- Lazzari, R. *Journal of Applied Crystallography* **35**, 406–421. ISSN: 1600-5767 (2002).
- Burle, J. *et al.* <[http : / / www . bornagainproject.org](http://www.bornagainproject.org)> (2018).
- Chourou, S. T., Sarje, A., Li, X. S., Chan, E. R. & Hexemer, A. *Journal of Applied Crystallography* **46**, 1781–1795. ISSN: 1600-5767 (2013).
- Sinha, S. K., Sirota, E. B., Garoff, S. & Stanley, H. B. *Physical Review B* **38**, 2297–2311 (1988).
- Rauscher, M., Salditt, T. & Spohn, H. *Physical Review B* **52**, 16855–16863 (1995).
- Renaud, G., Lazzari, R. & Leroy, F. *Surface Science Reports* **64**, 255–380. ISSN: 0167-5729 (2009).
- Vineyard, G. H. *Physical Review B* **26**, 4146–4159 (1982).
- Lazzari, R., Leroy, F. & Renaud, G. *Physical Review B* **76**, 125411 (2007).
- Als-Nielsen, J. & McMorrow, D. *Elements of modern X-ray physics* ISBN: 1119970156 (John Wiley & Sons, 2011).
- Narayanan, S., Lee, D. R., Guico, R. S., Sinha, S. K. & Wang, J. *Physical Review Letters* **94**, 145504 (2005).
- Lee, D. R. *et al.* *Applied Physics Letters* **88**, 153101 (2006).
- Babonneau, D., Camelio, S., Lantiat, D., Simonot, L. & Michel, A. *Physical Review B* **80**, 155446 (2009).
- Lee, B. *et al.* *Journal of Applied Crystallography* **41**, 134–142. ISSN: 0021-8898 (2008).
- Jiang, Z., Lee, D. R., Narayanan, S., Wang, J. & Sinha, S. K. *Physical Review B* **84**, 075440 (2011).
- Parratt, L. G. *Physical Review* **95**, 359–369 (1954).
- Gann, E., Caironi, M., Noh, Y.-Y., Kim, Y.-H. & McNeill, C. R. *Macromolecules* **51**, 2979–2987. ISSN: 0024-9297 (2018).
- Tolan, M. (1999).
- Henke, B. L., Gullikson, E. M. & Davis, J. C. *Atomic Data and Nuclear Data Tables* **54**, 181–342. ISSN: 0092-640X (1993).
- Alexander, H. *et al.* *Journal of Physics: Conference Series* **247**, 012007. ISSN: 1742-6596 (2010).